How to cite: *Angew. Chem. Int. Ed.* **2024**, *63*, e202410671
doi.org/10.1002/anie.202410671

Non-equilibrium Processes

Reduction-Induced Self-Propelled Oscillatory Motion of Perylenediimides on Water

Lara Rae Holstein, Nobuhiko J. Suematsu, Masayuki Takeuchi, Koji Harano, Taisuke Banno, and Atsuro Takai**

Abstract: The emergence of macroscopic self-propelled oscillatory motion based on molecular design has attracted continual attention in relation to autonomous systems in living organisms. Herein, a series of perylenediimides (PDIs) with various imide side chains was prepared to explore the impact of molecular design and alignment on the self-propelled motion at the air-water interface. When placed on an aqueous solution containing a reductant, a solid disk of neutral PDI was reduced to form the water-soluble, surface-active PDI dianion species, which induces a surface tension gradient in the vicinity of the disk for self-propelled motion. We found that centimeter-scale oscillatory motion could be elicited by controlling the supply rate of PDI dianion species through the reductant concentration and the structure of the imide side chains. Furthermore, we found that the onset and speed of the self-propelled motion could be changed by the crystallinity of PDI at the water surface. This design principle using π-conjugated molecules and their self-assemblies could advance self-propelled, non-equilibrium systems powered by chemical energy.

[*] L. R. Holstein, M. Takeuchi, A. Takai
Molecular Design and Function Group, National Institute for Materials Science (NIMS), 1-2-1 Sengen, Tsukuba, Ibaraki 305-0047, Japan
E-mail: TAKAI.Atsuro@nims.go.jp

L. R. Holstein, M. Takeuchi
Department of Materials Science and Engineering, Faculty of Pure and Applied Sciences, University of Tsukuba, 1-1-1 Tennodai, Tsukuba, Ibaraki 305-8577, Japan

N. J. Suematsu
School of Interdisciplinary Mathematical Sciences; Graduate School of Advanced Mathematical Sciences; Meiji Institute for Advanced Study of Mathematical Sciences (MIMS), Meiji University, 4-21-1, Nakano, Tokyo 164-8525, Japan
E-mail: suematsu@meiji.ac.jp

K. Harano
Center for Basic Research on Materials, National Institute for Materials Science (NIMS), 1-1 Namiki, Tsukuba, Ibaraki 305-0044, Japan

T. Banno
Department of Applied Chemistry, Faculty of Science and Technology, Keio University, 3-14-1 Hiyoshi, Kohoku-ku, Yokohama, Kanagawa 223-8522, Japan

Introduction

Animate objects transduce chemical energy into mechanical force, from which emerge autonomous rhythmic motions and spatial patterns, such as heartbeat and circadian activity. These autonomous behaviors are realized by a network of chemical reactions in a dissipative system, where hierarchical self-organized supramolecular assemblies convert molecular-level events into macroscopic ones.[1] In the last few decades, research on supramolecular systems chemistry that involves chemically-fueled reaction cycles has advanced tremendously, leading to the development of synthetic systems that exhibit oscillatory events of, for instance, self-assembling processes and color changes.[2] However, it remains a formidable challenge to explore synthetic systems capable of eliciting autonomous oscillatory motion at large length scales.

Meanwhile, inanimate, self-propelled objects have been extensively studied as a type of active matter, from organic to inorganic materials, some of which exhibit oscillatory motions.[3,4] Representative examples include organic solids, such as camphor, gels, and droplets containing surfactants that spontaneously move at the air-water or oil-water interface due to the Marangoni flow which is attributed to an anisotropic surface tension gradient in the vicinity of the objects.[5,6] It has also been reported that the continuous self-propelled motion of organic objects by the Marangoni flow is perturbed by a chemical reaction, resulting in oscillatory motion.[6] In the case of organic objects on the water surface, the driving force for the self-propelled motion is reduced by the chemical reaction; however, few systems are known in which the reaction product generates the driving force. Furthermore, most of these materials have been used in their bulk state consisting of random molecular orientations, paying little heed as to how consistent design of molecules, self-assembling processes, and chemical reactions may be combined to control macroscopic oscillatory motion.

To address these issues, we have employed a series of perylenediimide (PDI) molecules as motifs for self-propelled objects by taking advantage of a few key characteristics. Firstly, although PDI has a rigid and hydrophobic π-conjugated backbone, its hydrophilicity can be increased by introducing hydrophilic imide side chains.[7] Therefore, we

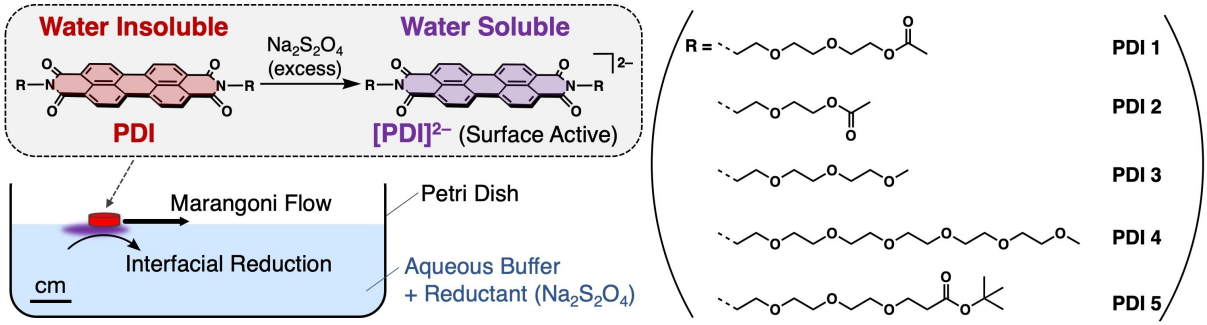

Figure 1. Schematic illustration of the reduction reaction of **PDI 1–5** at the water surface to form their dianion counterparts, which induces Marangoni flow.

envisioned that the interfacial properties of aqueous solutions, which govern the Marangoni effect, could be systematically tuned by the molecular design. Secondly, PDI is known to react with a reductant to form anionic species in water.[2g,8] Because the anionic species are more water-soluble than the neutral forms, the Marangoni flow can be altered by redox reactions. In addition, PDI is a well-known building block for supramolecular self-assembly,[9] therefore, the effect of molecular alignment of self-propelled objects at the interface on the autonomous motion could be explored. Considering these characteristics of PDIs, we report herein for the first time autonomous, centimeter-scale oscillatory motion of PDI solid disks induced by a reduction reaction at the air-water interface, with no background reactions, as illustrated in Figure 1. Importantly, we found that this macroscopic oscillatory motion was significantly affected by the imide side chains and the molecular alignment at the surface of the PDI disk.

Results and Discussion

Syntheses of PDI Derivatives and Their Redox Properties. We designed a series of PDIs (**PDI 1–5**) having oligo(ethylene glycol) chains with different terminal moieties at the imide positions, as shown in Figure 1. Compared to **PDI 1** and **PDI 3**, consisting of triethylene glycol chains, **PDI 4** with longer hexaethylene glycol chains is more hydrophilic, while **PDI 2** with shorter diethylene glycol chains and **PDI 5** with bulky *tert*-butoxycarbonyl (BOC) groups are more hydrophobic. All the PDIs were synthesized by a condensation reaction between 3,4,9,10-perylenetetracarboxylic dianhydride and the corresponding amines following a minor modification to a previously reported method.[10] Detailed experimental methods and characterization data (^{1}H NMR, ^{13}C NMR, and high-resolution mass analyses) are shown in Figures S1–S10 in the Supporting Information.

First, the redox properties of these PDIs were studied. Although **PDI 1–3** were hardly soluble in water, they dissolved in a *N*-cyclohexyl-2-aminoethanesulfonic acid (CHES) buffer solution at pH = 9.4 ± 0.2 containing excess sodium hydrosulfite ($Na_2S_2O_4$), a known reducing agent, yielding a reddish-purple solution. **PDI 4** was soluble in water both in the absence and presence of $Na_2S_2O_4$. This observation coupled with the UV/Vis absorption spectra of the resulting solutions of **PDI 1–4** in the presence of $Na_2S_2O_4$ (Figures 2 and S11a) were in good agreement with reports of analogous PDI dianion species, $[PDI]^{2-}$.[8a,11] In stark contrast, **PDI 5** remained almost insoluble in water despite the presence of $Na_2S_2O_4$, probably owing to the hydrophobic and sterically hindered BOC groups at the terminal of the imide side chains.

It is known that $[PDI]^{2-}$ reacts with dioxygen in air to revert to its original neutral state.[8a,c] However, when an aqueous solution of **PDI 1** in the presence of excess $Na_2S_2O_4$ in an open cuvette was stirred at 600 rpm at 25 °C, less than 10 % oxidation of $[\mathbf{PDI\ 1}]^{2-}$ was observed within 60 min, as shown in the inset of Figure S11b.[12] Similar results were also obtained for **PDI 2–4** under the same conditions. Therefore, the re-oxidation of $[PDI]^{2-}$ during the self-propelled motion, as will be discussed in the next section, did not need to be considered. Additionally, electrochemical measurements (cyclic voltammetry) of **PDI 1–5** showed that the first and second reduction potentials were almost identical among the PDIs (Figure S12). Thus, the electronic effects of the terminal structures of the oligo(ethylene glycol) imide side chains on the stability of $[PDI]^{2-}$ may be negligible.

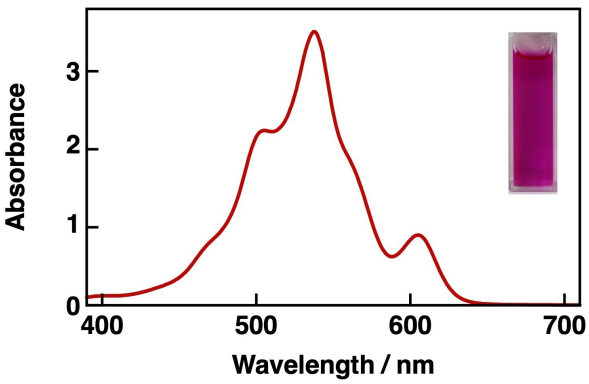

Figure 2. UV/Vis absorption spectra of **PDI 1** (60 μM) in the presence of $Na_2S_2O_4$ (46 mM) in a CHES buffer solution under air at 25 °C. The inset shows a photograph of the sample solution.

Swimming and Resting Motion of PDI 1. When a bulk solid of **PDI 1** was floated on a CHES buffer solution (pH = 9.4 ± 0.2) containing $Na_2S_2O_4$ (23 mM), periodic movements of swimming at a speed of less than 2 mm s^{-1} and resting were observed for over 30 s as shown in Movie S1.[13] Upon closer inspection, a dark purple solute corresponding to dissolved [**PDI 1**]$^{2-}$ could be seen diffusing from the bulk solid, eventually accumulating below the interface before the motion ceased. Similar behavior was also observed for a bulk solid of **PDI 3** (Movie S2). To study such macroscopic rhythmic motion in detail, we prepared PDI disks of uniform size (2 mm diameter with 0.5 mm thickness) to eliminate differences in motion dependent on the shape of the solid.[14] Because the **PDI 1** solid itself was too brittle to be molded by pressing, it was mixed with a polystyrene-isoprene elastomer and molded to obtain **PDI 1** elastomer disks (see Supporting Information for details). When placed on a CHES buffer solution containing $Na_2S_2O_4$ (23 mM) in a Petri dish (diameter: 60 mm, solution depth: 3 mm), the **PDI 1** disk exhibited oscillating self-propelled motion at a maximum speed of 2.0 mm s^{-1} and a frequency of 0.14 s^{-1} on average for over 300 s before coming to rest (Figure 3c and Movie S3). Unreacted **PDI 1** still remained in the disk after the disk was stopped, indicating that the amount of **PDI 1** (ca. 2 mg per disk) was sufficient and does not affect the self-propelled motion. The appearance of oscillatory motion of the **PDI 1** elastomer disk was similar to that of the **PDI 1** bulk solids, although the frequency and speed were different. Such oscillatory motion was not observed for a disk of pristine polystyrene-isoprene elastomer (Movie S4). Additionally, no motion of the **PDI 1** disk was observed in the absence of the $Na_2S_2O_4$, as shown in Movie S5. These results indicate that the motion was induced by the formation of [**PDI 1**]$^{2-}$ at the solid-liquid interface. Note that we also compared the self-propelled motion of the **PDI 1** disk at different depths of buffer solutions in a Petri dish (depths of 3 mm and 6 mm) and found no significant difference in the speed and duration. This result indicates that the main driving force of the PDI disks is the Marangoni flow, rather than other types of flow such as density-driven flow.

Spatiotemporal dynamics of the **PDI 1** disk could be altered by varying the concentration of $Na_2S_2O_4$. At low reductant concentrations, such as 2.3 mM, there was almost no movement (Figure 3a); when increased above 10 mM, slight but distinct self-propelled motion began to emerge (Figure 3b). Discontinuous intermittent motion was observed at both 23 mM and 46 mM, albeit with different behavioral consequences depending on the concentration. Unlike the slow, consistent oscillations over 300 s observed with 23 mM (Figure 3c), the 46 mM case saw significantly faster (maximum speed of 19 mm s^{-1}) yet shorter-lived, disk speeds that ceased within the first 100 s (Figure 3d). After a **PDI 1** disk on a $Na_2S_2O_4$ buffer solution (46 mM) came to a halt, a second **PDI 1** disk was added. No motion was observed for this second disk, however when the original disk was transferred to fresh reductant solution, self-propelled motion resumed as illustrated in Figure S13. When placed on an aqueous phase containing 92 mM of $Na_2S_2O_4$, the disks moved vigorously with a maximum speed of more than 11 mm s^{-1} only for the first few seconds before coming to a stop (Figure 3e). These results indicate that the rhythmic motion of **PDI 1** disks are highly dependent on the concentration of $Na_2S_2O_4$, and the cessation of motion is owed to the accumulation of [PDI]$^{2-}$ and possible oxidation to the insoluble PDI on the surface of the buffer solution. After the **PDI 1** disk had ceased moving, deposition of a thin film was observed at the surface of the buffer solution, and transmission electron microscopy (TEM) and electron diffraction confirmed that this material formed sheet-like crystals (Figure S14), indicating that [PDI]$^{2-}$ dispersed at the air-water interface tend to aggregate.

Autonomous Motion of the Other PDIs. We next investigated how the reduction-driven self-propelled motion of PDI elastomer disks changes depending on the imide side chain. Disks of **PDI 2** and **PDI 5** moved only slightly at a speed of less than 2 mm s^{-1} for the first few seconds and then stopped (Figures S15b and S15e). We infer that the low water solubility of [**PDI 2**]$^{2-}$ and [**PDI 5**]$^{2-}$ may have prevented sufficient reduction reactions and diffusion at the interface to induce self-propelled motion. A **PDI 3** disk exhibited intermittent swimming motion similar to **PDI 1**, as shown in Figure S15c and Movie S6, and a **PDI 4** disk swam slowly with ca. 0.5 mm s^{-1} for 15 min, as shown in Figure S15d and Movie S7. The apparent color change in the solution around the **PDI 4** disk attributed to the formation of [**PDI 4**]$^{2-}$ is presumably due to the significantly higher water solubility of [**PDI 4**]$^{2-}$ compared to the other PDIs.[15] These results suggest that designed solubility may be used to modulate the self-propelled motion.

Interfacial release of dianion species of **PDI 1–4** into the aqueous phase over time was followed by UV/Vis absorption spectroscopy to investigate the difference in the dissolution rate. For each of the PDI compounds, a 2 mm diameter PDI elastomer disk was placed on the surface of a stirred CHES buffer solution containing $Na_2S_2O_4$ (23 mM) in a cuvette. The dissolution kinetics could be monitored by the time profiles of the absorbance change (see Figure S16). The dissolution rate constant could be obtained by fitting to the Noyes-Whitney equation, which is a typical expression for the dissolution rate at the solid-liquid interface (see Supporting Information for details).[16] The resulting values are summarized in Table 1. We found that [**PDI 1**]$^{2-}$ and [**PDI 3**]$^{2-}$ had modest solubilities of 75 μM and 117 μM,

Table 1: Dissolution rate constant (k) and solubility of [PDI]$^{2-}$ in CHES buffer solutions, and surface tension (γ) of the solutions.

Compound	k/s^{-1}	Solubility/μM	γ /mN m^{-1} [b]
[**PDI 1**]$^{2-}$	(3.67 ± 0.04)×10^{-4}	75.0 ± 0.3	62.7 ± 0.6
[**PDI 2**]$^{2-}$	N/A[a]	0.36 ± 0.01	64.3 ± 1.7
[**PDI 3**]$^{2-}$	(5.05 ± 0.03)×10^{-4}	116.8 ± 0.3	51.3 ± 2.9
[**PDI 4**]$^{2-}$	(5.20 ± 0.11)×10^{-4}	341.5 ± 2.8	54.6 ± 0.1
[**PDI 5**]$^{2-}$	N/A[a]	N/A	69.4 ± 0.6

[a] The dissolution rate constant could not be calculated for [**PDI 2**]$^{2-}$ and [**PDI 5**]$^{2-}$ because they are nearly insoluble in water. [b] The γ values were measured for solutions containing PDIs (60 μM) and $Na_2S_2O_4$ (23 mM). The γ value of a CHES buffer solution with $Na_2S_2O_4$ (23 mM) was 69.6 ± 0.4 mN m^{-1}.

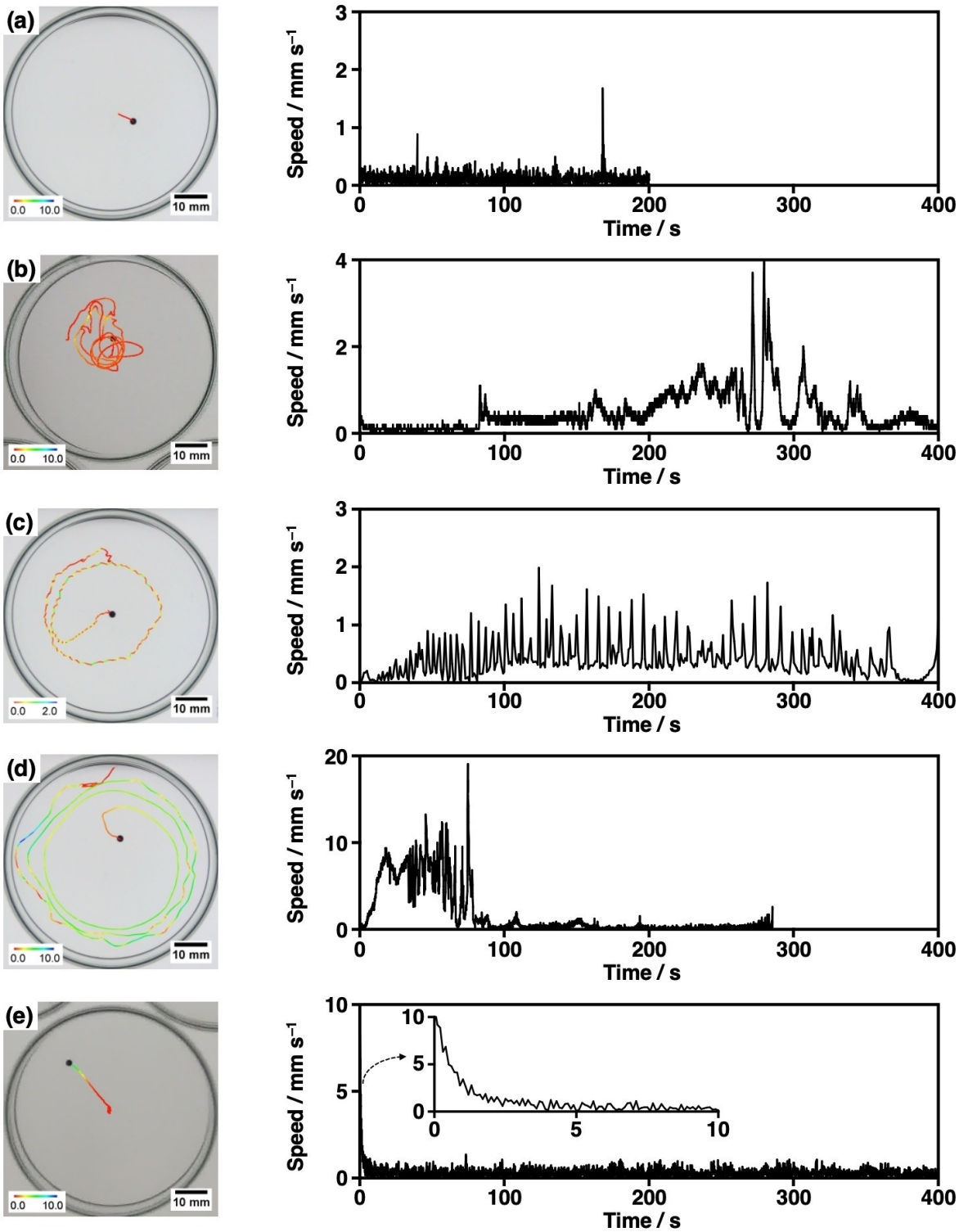

Figure 3. Top view of the trajectory (left) and speed profile (right) of **PDI 1** disks on a CHES buffer solution containing various concentrations of $Na_2S_2O_4$: (a) 2.3 mM, (b) 11 mM, (c) 23 mM, (d) 46 mM, and (e) 92 mM. The color of the trajectory indicates the speed of the disk in mm s^{-1}.

respectively, while [**PDI 2**]$^{2-}$ reached a poor solubility of 0.36 μM. No dianion spectral peaks could be observed for **PDI 5** owing to its insolubility under these conditions. On the other hand, [**PDI 4**]$^{2-}$ exhibited the highest solubility of 342 μM, which was consistent with the appearance of an intense reddish-purple solution as shown in Figure S15d and Movie S7. The respective dissolution rate constants followed a similar order as the solubility, although it was not possible to accurately determine the rate constants for [**PDI 2**]$^{2-}$ and [**PDI 5**]$^{2-}$ due to their poor solubility. These results, coupled

with our observations of different swimming behaviors, indicate that there is an optimum region of solubility, or dissolution rate, in water where the self-propelled motion of the disk is maximized.

We have also studied the extent of surface tension change upon formation of the respective $[PDI]^{2-}$ in buffer solutions, because the self-propelled motion of the PDI disk is induced by the Marangoni flow, which is attributed to the surface tension gradient around the disk. As shown in Table 1, the surface tension (γ) of CHES buffer solutions of **PDI 1**, **PDI 2**, **PDI 3**, and **PDI 4** dianion species (60 μM) was found to be significantly lower than that of pristine buffer solution at 69.6 mN m^{-1}. The γ value of a $[$**PDI 2**$]^{2-}$ solution at 60 μM (64.3 mN m^{-1}) obtained by sonication was comparable to that of a $[$**PDI 1**$]^{2-}$ solution (62.7 mN m^{-1}). However, the low solubility at the solid-liquid interface did not result in a sufficient surface tension gradient; consequently, **PDI 2** disks showed little self-propelled motion. **PDI 5** and its dianion could not be effectively dissolved even by sonication. As a result, its γ value (69.4 mN m^{-1}) was measured to be almost the same as that of the CHES buffer solution (69.6 mN m^{-1}). The γ values were also measured as a function of $[PDI]^{2-}$ concentration for **PDIs 1–4**. As shown in Figure S17, the γ value tends to decrease linearly with increasing $[PDI]^{2-}$ concentrations. Inflection points were observed at 70 μM and 2 μM for $[$**PDI 1**$]^{2-}$ and $[$**PDI 4**$]^{2-}$, respectively, as critical aggregation concentrations were reached. These results are consistent with the TEM results (Figure S14), in which aggregate formation derived from $[$**PDI 1**$]^{2-}$ was observed at the air-water interface.

Mechanism of Rhythmic Motion of PDIs. We have demonstrated the interfacial reduction of PDI can be applied to induce rhythmic self-propelled motion. Unlike typical self-propelled systems, such as camphor, where the disk itself is composed of surface-active species, our system requires an activating process that converts surface-inactive PDI molecules to surface-active $[PDI]^{2-}$. We attribute variations in the type of self-propelled behavior to local concentration conditions around each disk; thus, the mechanism can be described by considering three main cases relating to dianion supply. As depicted in Figure 4a, at lower supply rates of $[PDI]^{2-}$ (Case 1), the net force acting on the disk is too small to induce an observable degree of motion. At moderate supply rates of $[PDI]^{2-}$ (Case 2), the PDI disk obtains a sufficient driving force from the resulting surface tension gradient. At higher supply rates of $[PDI]^{2-}$ (Case 3), the gradient around the disk is too low to induce motion, because all sides are saturated with $[PDI]^{2-}$.

We surmise that the rhythmic self-propelled motion of **PDI 1** and **PDI 3** disks was observed in a state of delicately balanced conditions between Case 1 and Case 2. At the beginning, the disk starts to move via a positive feedback process, where the inhomogeneity of $[PDI]^{2-}$ induces a surface tension gradient that causes Marangoni flow (swimming).[6c] The motion of the disk also induces inhomogeneity as a relatively higher concentration of $Na_2S_2O_4$ emerges in front of the moving disk as a consequence of local reductant consumption behind the disk. Eventually, the production rate of $[PDI]^{2-}$ at the front becomes

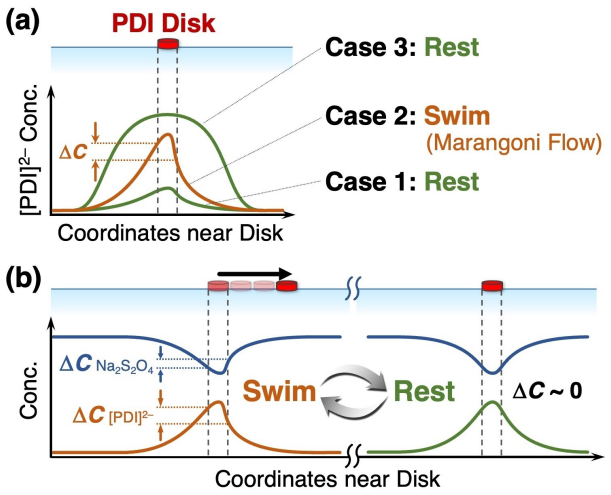

Figure 4. (a) Schematic diagram depicting three $[PDI]^{2-}$ concentration profile scenarios. (b) Mechanism of the oscillatory motion of PDIs on water upon reduction.

sufficiently high, which decreases the surface tension, resulting in restored symmetry of the forces acting on the disk as it slows to a stop (rest). During the rest, $[PDI]^{2-}$ concentration increases over time and the disk starts to move again, as depicted in Figure 4b. Here, the slight inhomogeneity of $[PDI]^{2-}$ might remain, thus the movement direction becomes almost the same as the previous motion.[17]

Minimal self-propelled movement of **PDI 2** with its short diethylene glycol side chains and **PDI 5** with its bulky, hydrophobic BOC moieties can be described by Case 1, where the concentrations of their dianion species are not high enough to induce a sufficient surface tension gradient. By contrast, $[$**PDI 4**$]^{2-}$, possessing high solubility coupled with low surface tension values, exhibited only slow self-propelled motion, which corresponds to Case 3. These results demonstrate how the parameters governing the supply of surface-active species, such as variations in the chemical structure of the imide side chains of PDIs and reductant concentrations, can be used to control the behavior of self-propelled PDI disks.

Effect of Molecular Alignment of PDIs on Self-Propelled Motion. Finally, we investigated how the molecular alignment of PDIs could affect the self-propelled behavior. As a representative example, we prepared thin films of **PDI 1** by drop-casting chloroform solution onto 3 mm diameter (0.2 mm thick) polyimide disks, followed by an annealing treatment (Figure 5a; see Supporting Information for details).[18] Thermogravimetric (TG) analysis showed that **PDI 1** is thermally stable up to 310 °C (Figure S18a) and differential scanning calorimetry (DSC) results indicated isotropic melting at 303 °C (Figure S18b). Crystalline domains were formed upon heating to 305 °C and subsequent cooling of the drop-cast **PDI 1** coated polyimide disks; Meanwhile, those left at room temperature maintained a mostly isotropic phase, as observed by polarized optical microscopy (POM; Figure 5b). The difference in crystallinity

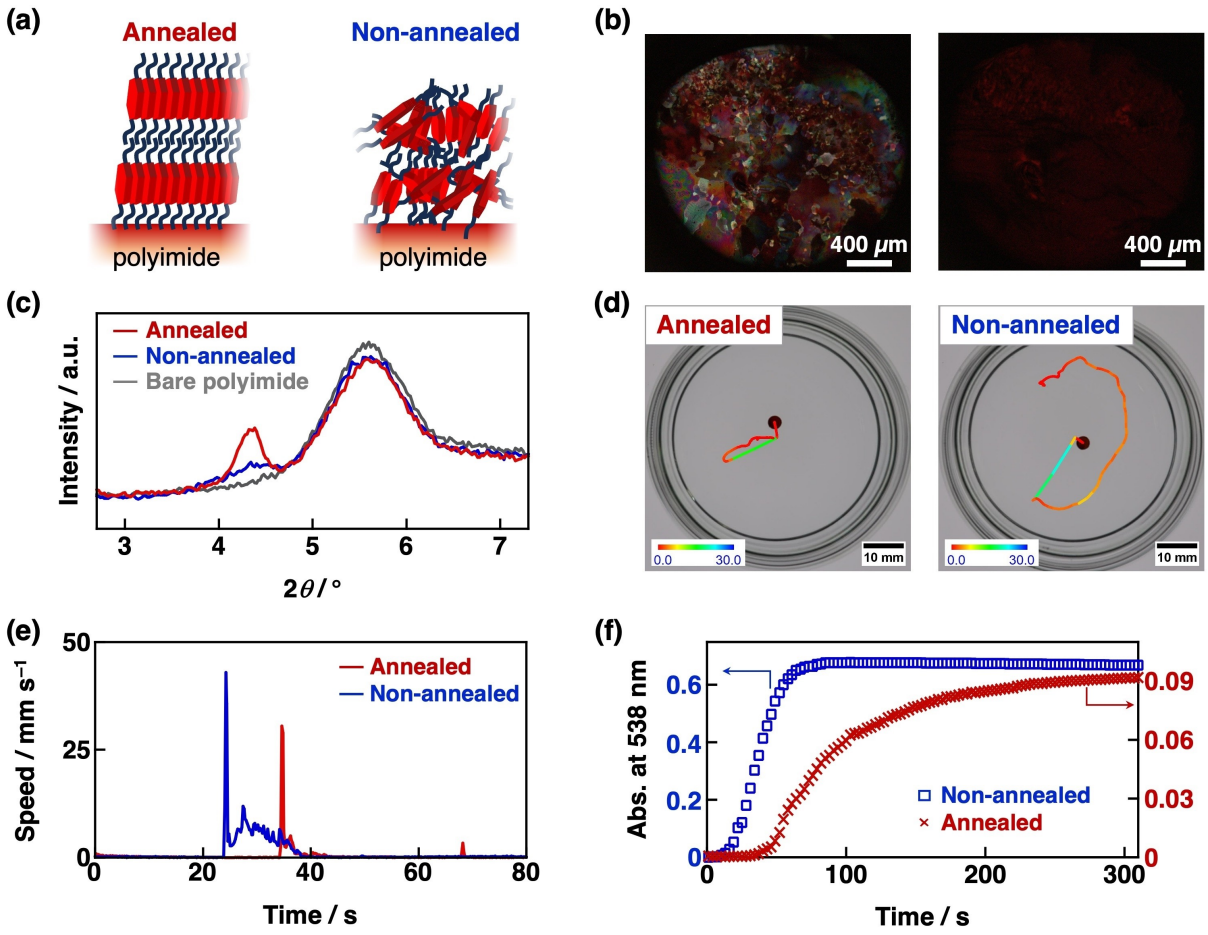

Figure 5. (a) Schematic illustration of the assembled structure of PDI with and without annealing. (b) POM images of **PDI 1** coated polyimide disks with (left) and without (right) annealing at 305 °C. (c) XRD profiles of **PDI 1** drop-cast onto polyimide with (red line) and without (blue line) annealing. (d) Typical trajectory and (e) The corresponding speed profiles of **PDI 1** disks with and without annealing on a CHES buffer solution containing $Na_2S_2O_4$ (23 mM). The color of the trajectory indicates the speed of the disk in mm s^{-1}. (f) Time profiles of the absorbance changes at 538 nm upon addition of **PDI 1** disks with (red crosses) and without (blue squares) annealing on a stirred CHES buffer solution containing $Na_2S_2O_4$ (23 mM).

between the annealed and non-annealed disks was also supported by X-ray diffraction (XRD) measurements (Figure 5c). The annealed sample displayed a peak at $2\theta = 4.3°$ (2.04 nm) which roughly corresponds to the length of **PDI 1** along the long axis, indicating vertical lamellar stacking.[19] On the other hand, the intensity of the respective peak of the non-annealed film was much smaller, indicating that **PDI 1** is disordered in the film.

Distinct differences in self-propelled motion emerged when we compared the behaviors of annealed and non-annealed **PDI 1** films on polyimide for at least 8 different samples (Figures 5d and 5e). Disks coated with annealed **PDI 1** film displayed self-propelled motion with maximum speeds averaging 33 mm s^{-1} upon contact with $Na_2S_2O_4$ buffer solution (Movie S8). By contrast, non-annealed disks exhibited faster self-propelled motion (44 mm s^{-1} on average), depositing a thick, dark purple solution indicative of the rapid release of $[\mathbf{PDI\ 1}]^{2-}$ around the disk (Movie S9). We also observed that the onset of motion took longer for annealed samples (34 s) than for their non-annealed counterparts (22 s). This observation was reinforced by UV/Vis absorption spectroscopy of $[\mathbf{PDI\ 1}]^{2-}$ release rate (Figure 5f), which was monitored by placing a **PDI 1** disk on the surface of a stirred CHES buffer solution containing $Na_2S_2O_4$ (23 mM). The time profile of $[\mathbf{PDI\ 1}]^{2-}$ generated from the annealed sample displayed a considerable waiting period for ca. 40 s before the absorbance increased, in addition to the lower absorbance during the first 300 seconds compared to the non-annealed sample. Large, rod-like domains were observed when the annealed sample was viewed under scanning electron microscopy (SEM) as shown in Figure S18c. Therefore, the altered self-propelled behavior is probably due to the higher crystallinity of the annealed sample that significantly decreased the total concentration of $[\mathbf{PDI\ 1}]^{2-}$ released into the bulk phase. The annealed sample exhibited minimal oscillatory motion, likely because the low concentration of $[\mathbf{PDI\ 1}]^{2-}$ around the disk fell under Case 1, where a sufficient surface tension gradient for Marangoni flow was not induced (Figure 4a). These results demonstrate how molecular alignment of PDI molecules at

the interface with water, even a partial alignment, can be used to modulate macroscopic self-propelled motion by influencing the supply rate. The effect of longer-range, anisotropic PDI alignment on their direction and speed of self-propelled motion of the disk is currently under study in our groups.

Conclusions

In summary, we have shown an autonomous, centimeter-scale oscillatory motion induced by the generation of surface-active dianion species of perylenediimide (PDI) through an interfacial reduction reaction. We demonstrated how the solubility, and hence the supply rate, of surface-active species, as well as the surface tension of the buffer solution, could be modulated by variations in the side chains of the PDI π-scaffold and in the reductant concentration. Further modulation of the self-propelled motion on water was achieved by changing the molecular alignment of PDI films at the solid-water interface through an annealing treatment. The design principle of self-propelled objects based on π-conjugated molecules and their self-assemblies presented here will pave the way to create supramolecular systems under non-equilibrium conditions that achieve desired motion using chemical energy.

Acknowledgements

We acknowledge Ms. Izumi Matsunaga (NIMS) for her assistance with the experiments, especially with the syntheses of the PDI compounds, Dr. Takanobu Hiroto (NIMS) for his assistance with the XRD measurements, and Dr. Takeshi Yasuda (NIMS) for his assistance to prepare thin film samples. A.T. is grateful for financial support from JSPS (a Grant-in-Aid for Scientific Research (C); JP23K04725), the Izumi Science and Technology Foundation, and the Inamori Foundation. N.J.S. is grateful for financial support from JSPS (a Grant-in-Aid for Scientific Research (C); JP23K03347 and (B); JP21H01004, JP20H02712, and JP20H01871). We also thank support from a JSPS Grant-in-Aid for Transformative Research Areas (A) "Materials Science of Meso-Hierarchy" (JP24H01734 to A.T. and JP23H04874 to K.H.) and ARIM of MEXT (JPMXP1223NM5141 and JPMXP1224NM5109).

Conflict of Interest

There are no conflicts to declare.

Data Availability Statement

The data that support the findings of this study are available in the supplementary material of this article.

Keywords: Perylene dyes · Nonequilibrium processes · Reduction · Marangoni flow · Oscillatory motion

[1] a) A. Goldbeter, *Biochemical Oscillations and Cellular Rhythms: The Molecular Bases of Periodic and Chaotic Behaviour*, Cambridge University Press, Cambridge, UK, **1996**; b) E. Karsenti, *Nat. Rev. Mol. Cell Biol.* **2008**, *9*, 255; c) B. A. Grzybowski, *Chemistry in Motion, Reaction-Diffusion Systems for Micro- and Nanotechnology*, John Wiley & Sons, Chichester, UK, **2009**; d) J.-M. Lehn, *Angew. Chem. Int. Ed.* **2013**, *52*, 2836; e) P. K. Hashim, J. Bergueiro, E. W. Meijer, T. Aida, *Prog. Polym. Sci.* **2020**, *105*.

[2] a) I. Lagzi, B. Kowalczyk, D. W. Wang, B. A. Grzybowski, *Angew. Chem. Int. Ed.* **2010**, *49*, 8616; b) E. Mattia, S. Otto, *Nat. Nanotechnol.* **2015**, *10*, 111; c) S. N. Semenov, A. S. Y. Wong, R. M. van der Made, S. G. J. Postma, J. Groen, H. W. H. van Roekel, T. F. A. de Greef, W. T. S. Huck, *Nat. Chem.* **2015**, *7*, 160; d) S. N. Semenov, L. J. Kraft, A. Ainla, M. Zhao, M. Baghbanzadeh, V. E. Campbell, K. Kang, J. M. Fox, G. M. Whitesides, *Nature* **2016**, *537*, 656; e) G. Ashkenasy, T. M. Hermans, S. Otto, A. F. Taylor, *Chem. Soc. Rev.* **2017**, *46*, 2543; f) S. A. P. van Rossum, M. Tena-Solsona, J. H. van Esch, R. Eelkema, J. Boekhoven, *Chem. Soc. Rev.* **2017**, *46*, 5519; g) J. Leira-Iglesias, A. Tassoni, T. Adachi, M. Stich, T. M. Hermans, *Nat. Nanotechnol.* **2018**, *13*, 1021; h) S. Dhiman, S. J. George, *Bull. Chem. Soc. Jpn.* **2018**, *91*, 687; i) S. N. Semenov, in *Out-of-Equilibrium (Supra)molecular Systems and Materials* (Eds.: N. Giuseppone, A. Walther), Wiley-VCH, Weinheim, Germany, **2021**, pp. 91; j) F. Sheehan, D. Sementa, A. Jain, M. Kumar, M. Tayarani-Najjaran, D. Kroiss, R. V. Ulijn, *Chem. Rev.* **2021**, *121*, 13869; k) M. G. Howlett, A. H. J. Engwerda, R. J. H. Scanes, S. P. Fletcher, *Nat. Chem.* **2022**, *14*, 805; l) M. ter Harmsel, O. R. Maguire, S. A. Runikhina, A. S. Y. Wong, W. T. S. Huck, S. R. Harutyunyan, *Nature* **2023**, *621*, 87; m) B. Dúzs, I. Lagzi, I. Szalai, *ChemSystemsChem* **2023**, *5*, e202200032.

[3] a) S. Ramaswamy, *Annu. Rev. Condens. Matter Phys.* **2010**, *1*, 323; b) W. Wang, W. Duan, S. Ahmed, T. E. Mallouk, A. Sen, *Nano Today* **2013**, *8*, 531; c) S. Sánchez, L. Soler, J. Katuri, *Angew. Chem. Int. Ed.* **2015**, *54*, 1414; d) Y. Tu, F. Peng, A. Adawy, Y. Men, L. K. E. A. Abdelmohsen, D. A. Wilson, *Chem. Rev.* **2016**, *116*, 2023; e) P. Illien, R. Golestanian, A. Sen, *Chem. Soc. Rev.* **2017**, *46*, 5508; f) *Self-organized Motion: Physicochemical Design based on Nonlinear Dynamics* (Eds.: S. Nakata, V. Pimienta, I. Lagzi, H. Kitahata, N. J. Suematsu), The Royal Society of Chemistry, Cambridge, UK, **2018**; g) Z.-Z. Nie, M. Wang, H. Yang, *Commun. Chem.* **2024**, *7*, 58.

[4] a) S. Nakata, M. Murakami, *Langmuir* **2010**, *26*, 2414; b) T. Ikegami, Y. Kageyama, K. Obara, S. Takeda, *Angew. Chem. Int. Ed.* **2016**, *55*, 8239; c) S. Fujii, S. Yusa, Y. Nakamura, *Adv. Funct. Mater.* **2016**, *26*, 7206; d) Y. Tu, F. Peng, X. Sui, Y. Men, P. B. White, J. C. M. van Hest, D. A. Wilson, *Nat. Chem.* **2017**, *9*, 480; e) A. Altemose, M. A. Sánchez-Farrán, W. Duan, S. Schulz, A. Borhan, V. H. Crespi, A. Sen, *Angew. Chem. Int. Ed.* **2017**, *56*, 7817; f) R. Tenno, Y. Gunjima, M. Yoshii, H. Kitahata, J. Gorecki, N. J. Suematsu, S. Nakata, *J. Phys. Chem. B* **2018**, *122*, 2610; g) Y. Matsuda, K. Ikeda, Y. Ikura, H. Nishimori, N. J. Suematsu, *J. Phys. Soc. Jpn.* **2019**, *88*, 093002; h) C. Zhou, N. J. Suematsu, Y. Peng, Q. Wang, X. Chen, Y. Gao, W. Wang, *ACS Nano* **2020**, *14*, 5360; i) S. Arnaboldi, G. Salinas, A. Karajic, P. Garrigue, T. Benincori, G. Bonetti, R. Cirilli, S. Bichon, S. Gounel, N. Mano, A. Kuhn, *Nat. Chem.* **2021**, *13*, 1241; j) G. Vantomme, L. C. M. Elands, A. H. Gelebart, E. W. Meijer, A. Y. Pogromsky, H. Nijmeijer, D. J. Broer, *Nat. Mater.* **2021**, *20*, 1702; k) R. Yoshida, *Polym. J.* **2022**, *54*, 827.

[5] a) C. Tomlinson, *Proc. R. Soc. London* **1862**, *11*, 575; b) S. Nakata, Y. Iguchi, S. Ose, M. Kuboyama, T. Ishii, K. Yoshikawa, *Langmuir* **1997**, *13*, 4454; c) Y. Ikezoe, G. Washino, T. Uemura, S. Kitagawa, H. Matsui, *Nat. Mater.* **2012**, *11*, 1081; d) T. Bánsági, M. M. Wrobel, S. K. Scott, A. F. Taylor, *J. Phys. Chem. B* **2013**, *117*, 13572; e) J. M. P. Gutierrez, T. Hinkley, J. W. Taylor, K. Yanev, L. Cronin, *Nat. Commun.* **2014**, *5*, 5571; f) J. Cejková, T. Banno, M. M. Hanczyc, F. Stepánek, *Artif. Life* **2017**, *23*, 528; g) M. J. Cheng, G. Q. Zhu, L. Li, S. Zhang, D. Q. Zhang, A. J. C. Kuehne, F. Shi, *Angew. Chem. Int. Ed.* **2018**, *57*, 14106; h) C. H. Meredith, P. G. Moerman, J. Groenewold, Y. J. Chiu, W. K. Kegel, A. van Blaaderen, L. D. Zarzar, *Nat. Chem.* **2020**, *12*, 1136; i) Y. F. Yano, H. Tada, E. Arakawa, W. Voegeli, T. Ina, T. Uruga, T. Matsushita, *J. Phys. Chem. Lett.* **2020**, *11*, 6330; j) A. van der Weijden, M. Winkens, S. M. C. Schoenmakers, W. T. S. Huck, P. A. Korevaar, *Nat. Commun.* **2020**, *11*, 4800; k) D. Babu, N. Katsonis, F. Lancia, R. Plamont, A. Ryabchun, *Nat. Chem. Rev.* **2022**, *6*, 377; l) T. Kojima, H. Kitahata, K. Asakura, T. Banno, *Cell Rep. Phys. Sci.* **2023**, *4*, 101222; m) Y. Sumino, R. Yamashita, K. Miyaji, H. Ishikawa, M. Otani, D. Yamamoto, E. Okita, Y. Okamoto, M. P. Krafft, K. Yoshikawa, A. Shioi, *Sci. Rep.* **2023**, *13*, 12377; n) S. W. Song, S. Lee, J. K. Choe, A. C. Lee, K. Shin, J. W. Kang, G. Kim, H. Yeom, Y. Choi, S. Kwon, J. Kim, *Nat. Commun.* **2023**, *14*, 3597.

[6] a) S. Nakata, M. Yoshii, S. Suzuki, R. Yoshida, *Langmuir* **2014**, *30*, 517; b) N. J. Suematsu, Y. Mori, T. Amemiya, S. Nakata, *J. Phys. Chem. Lett.* **2016**, *7*, 3424; c) N. J. Suematsu, S. Nakata, *Chem. Eur. J.* **2018**, *24*, 6308; d) T. Fujino, M. Matsuo, V. Pimienta, S. Nakata, *J. Phys. Chem. Lett.* **2023**, *14*, 9279; e) M. Matsuo, K. Ejima, S. Nakata, *J. Colloid Interface Sci.* **2023**, *639*, 324; f) G. Zhu, S. Zhang, G. Lu, B. Peng, C. Lin, L. Zhang, F. Shi, Q. Zhang, M. Cheng, *Angew. Chem. Int. Ed.* **2024**, *63*, e202405287.

[7] M. M. Sun, K. Müllen, M. Z. Yin, *Chem. Soc. Rev.* **2016**, *45*, 1513.

[8] a) E. Shirman, A. Ustinov, N. Ben-Shitrit, H. Weissman, M. A. Iron, R. Cohen, B. Rybtchinski, *J. Phys. Chem. B* **2008**, *112*, 8855; b) Y. Jiao, K. Liu, G. Wang, Y. Wang, X. Zhang, *Chem. Sci.* **2015**, *6*, 3975; c) J. Leira-Iglesias, A. Sorrenti, A. Sato, P. A. Dunne, T. M. Hermans, *Chem. Commun.* **2016**, *52*, 9009; d) C. Chen, Z. Guan, *Chem. Eur. J.* **2023**, *29*, e202300347; e) C. F. Chen, J. S. Valera, T. B. M. Adachi, T. M. Hermans, *Chem. Eur. J.* **2023**, *29*, e202202849.

[9] a) M. R. Wasielewski, *Acc. Chem. Res.* **2009**, *42*, 1910; b) F. Würthner, C. R. Saha-Möller, B. Fimmel, S. Ogi, P. Leowanawat, D. Schmidt, *Chem. Rev.* **2016**, *116*, 962.

[10] a) H. Langhals, *Heterocycles* **1995**, *40*, 477; b) C. Huang, S. Barlow, S. R. Marder, *J. Org. Chem.* **2011**, *76*, 2386; c) Y. He, S. Savagatrup, L. D. Zarzar, T. M. Swager, *ACS Appl. Mater. Interfaces* **2017**, *9*, 7804.

[11] The corresponding radical anions, $[PDI]^{\bullet-}$ should be formed transiently, but we could not observe them under the experimental conditions owing to the immediate transformation into $[PDI]^{2-}$ with the excess reductant.

[12] After about one day of standing, the color of the solution became clear and a red solid was observed precipitating on the surface of the solution. The recovered solid was dissolved in $CDCl_3$ for ^1H NMR measurement, and it was determined to be **PDI 1** that had returned to the neutral state.

[13] We chose a CHES buffer solution at pH 9.4 ± 0.2 because the $Na_2S_2O_4$ aqueous solution and $[PDI]^{2-}$ were stable under these basic conditions. We confirmed that the PDI disks also swam in HEPES buffer solution at lower pH 8.2 ± 0.2, but the experimental results varied due to the low stability of $[PDI]^{2-}$ as well as the reductant.

[14] a) J. P. Gong, S. Matsumoto, M. Uchida, N. Isogai, Y. Osada, *J. Phys. Chem.* **1996**, *100*, 11092; b) H. Kitahata, K. Iida, M. Nagayama, *Phys. Rev. E* **2013**, *87*, 010901; c) H. Kitahata, Y. Koyano, *J. Phys. Soc. Jpn.* **2020**, *89*, 094001; d) Y. Koyano, H. Kitahata, *Phys. Rev. E* **2021**, *103*, 012202.

[15] Note that although the other PDI disks showed less visible color change of the solute than the **PDI 4** disk, when the solutions around the disks were monitored from the side or left standing even after the disks stopped, a dark purple solute corresponding to dissolved $[PDI]^{2-}$ was clearly observed diffusing from underneath the disk.

[16] H. Takeuchi, in *Powder Technology Handbook*, 4th ed. (Eds.: K. Higashitani, H. Makino, S. Matsusaka), CRC Press, Boca Raton, US, **2019**, pp. 171.

[17] The oxidation of $[PDI]^{2-}$ by dioxygen in air at the air-water interface and the formation of aggregates, which is not soluble in water, may also be one of the reasons for the cessation of movement.

[18] We employed a polyimide film owing to its thermal stability up to 400 °C or higher. The diameter of the disks was increased for improved ease of handling, and the amount of PDI (20 μg each) to drop-cast was unified.

[19] a) S. Tatemichi, M. Ichikawa, T. Koyama, Y. Taniguchi, *Appl. Phys. Lett.* **2006**, *89*, 112108; b) T. N. Krauss, E. Barrena, X. N. Zhang, D. G. de Oteyza, J. Major, V. Dehm, F. Würthner, L. P. Cavalcanti, H. Dosch, *Langmuir* **2008**, *24*, 12742; c) T. Yasuda, K. Sakamoto, *Org. Electron.* **2018**, *62*, 429.

Manuscript received: June 6, 2024
Accepted manuscript online: July 31, 2024
Version of record online: October 2, 2024